

Fréchet Power-Scenario Distance: A Metric for Evaluating Generative AI Models across Multiple Time-Scales in Smart Grids

Yuting Cai, *Student Member, IEEE*, Shaohuai Liu, *Student Member, IEEE*, Chao Tian, *Senior Member, IEEE*, Le Xie, *Fellow, IEEE*

Abstract—Generative artificial intelligence (AI) models in smart grids have advanced significantly in recent years due to their ability to generate large amounts of synthetic data, which would otherwise be difficult to obtain in the real world due to confidentiality constraints. A key challenge in utilizing such synthetic data is how to assess the data quality produced from such generative models. Traditional *Euclidean distance-based* metrics only reflect pair-wise relations between two individual samples, and could fail in evaluating quality differences between groups of synthetic datasets. In this work, we propose a novel metric based on the *Fréchet Distance (FD)* estimated between two datasets in a learned feature space. The proposed method evaluates the quality of generation from a distributional perspective. Empirical results demonstrate the superiority of the proposed metric across timescales and models, enhancing the reliability of data-driven decision-making in smart grid operations.

Index Terms—Generative model, synthetic data evaluation, machine learning, energy data

I. INTRODUCTION

GENERATIVE models in the electric energy sector have been an active field of research in the past few years, thanks to their potential to create realistic and diverse scenarios for system planning, reliability assessment, and renewable energy integration—ultimately enhancing grid resilience and operational efficiency. These models, such as Generative Adversarial Networks (GANs), allow researchers to access much larger sets of synthetic data across multiple time scales that would otherwise be unavailable due to confidentiality constraints [1]. In contrast to traditional methods that involve creating synthetic power networks and subsequently using commercial-grade simulation software to generate electrical measurement variables [2], these generative approaches leverage a data-driven methodology. They produce large volumes of synthetic electrical data by utilizing historical electrical measurements in a computationally efficient manner.

While these generative models hold great potential for a wide range of power system applications, a central question remains largely unexplored: What would be a fair and robust metric to evaluate the quality of various generative techniques in creating synthetic power system data across multiple time

resolutions? Conventionally, evaluation methods are based on Euclidean metrics between pairs of samples (signals), such as Mean Squared Error (MSE) and Mean Absolute Percentage Error (MAPE) [3]–[6]. However, these methods are susceptible to the selection of samples, leading to inconsistent evaluations. Moreover, the sample-by-sample comparison approach poses challenges when evaluating datasets produced by generative models, where the distributional properties of the datasets are more critical.

As an alternative, distribution-based comparison methods, such as Fréchet Distance (FD), which can capture the broader distributional characteristics of generative models, have been explored in previous work [7]. However, applying FD directly at the data level may not effectively capture the similarity between datasets. Other approaches have opted for task-specific metrics that involve statistical analysis of task-based parameters. For instance, the number of zeros is employed as a task-specific indicator to assess the quality of voltage sag generation in [8]. Similarly, the indicators used to detect anomalies in electricity consumption include residential stimulus allocation, residential tariff allocation, and SME (Small and Medium-sized Enterprise) allocation in [9]. However, these approaches introduce inconsistencies, as the evaluation criteria vary across tasks. The variability makes it challenging to achieve a unified understanding of a model’s overall performance or to establish standardized benchmarks, potentially leading to biased assessments.

Building on insights from computer vision research, where generative model evaluation has been extensively explored, we investigate methods that could establish more reliable evaluation standards. One such approach is the Inception Score (IS) [10], which was initially adopted to assess the quality and diversity of generated images using a pre-trained Inception network. However, IS faced criticism for its inability to detect the mode collapse of the generative model, where the model produces a limited variety of outputs or concentrates on only a few modes within the distribution, resulting in potential failures across various scenarios [11]. The Fréchet Inception Distance (FID) was proposed to overcome these limitations. FID computes the Fréchet distance between the distributions of real and generated images in a vectorized feature space mapped by a pre-trained Inception network, namely Inception v3. This metric considers both the mean and covariance of the feature space of real and generated data distributions, making it more sensitive to variations in both quality and diversity while

Yuting Cai, Shaohuai Liu and Chao Tian are with Department of Electrical and Computer Engineering, Texas A&M University, College Station, TX, 77843 USA (e-mail: cyuting@tamu.edu; liushaohuai5@tamu.edu; chao.tian@tamu.edu). Le Xie is with the John A. Paulson School of Engineering and Applied Sciences, Harvard University, Boston, MA 02134 USA (e-mail: xie@seas.harvard.edu)

closely aligning with human perception [12]. [13] suggests using Kernel Inception Distance (KID), which implements Maximum Mean Discrepancy (MMD) with kernel functions applied to the feature space of the Inception model can further improve the metric performance compared to FID. Unlike FID, which can suffer from estimator bias. KID provides an unbiased estimate, ensuring stable evaluation, particularly for small sample datasets. However, this approach is highly dependent on the choice of kernel functions, with different kernels potentially leading to inconsistent results.

Inspired by the success of the FID metric, in this paper we aim to develop a robust metric that could work in the context of multi-time-scale generative data sets in smart grids. The challenge that arises in adapting FID for this context are as follows: (1) The original FID feature extractor, Inception v3, is optimized primarily to capture image-specific features, making it potentially unsuitable for power system data; (2) FID metric is developed based on the ImageNet dataset, which contains over 14 million images across 1,000 categories as a comprehensive benchmark for most image generation tasks [14], whereas there is no standardized dataset of comparable scope and diversity for power systems; (3) Inception V3 model requires a fixed input resolution of 299x299 pixels, which is incompatible with the multi-resolution and multi-duration characteristics inherent to power system data.

To address these three challenges, we (1) train a new feature extraction model to capture both spatial and temporal features critical for power system data, enhancing its performance on such datasets; (2) collect comprehensive data set which, to the best of our knowledge, captures the major synthetic tasks associated with power systems; and (3) design a hierarchical structure composed of multiple feature extractors to handle multi-resolution datasets, enabling features from shorter timescales to be effectively integrated into models operating at longer timescales.

The key contributions of this paper are suggested as follows:

- 1) **A hierarchy multi-resolution feature extraction network:** We present a novel network design where multiple feature extractors are trained to handle data at different time resolutions and are connected in a hierarchical structure. This approach enables data of varying resolutions to be accommodated within the model, ensuring that features from shorter timescales are effectively transferred to longer timescales, thereby enhancing the model's ability to capture the complex temporal dynamics inherent in power systems.
- 2) **A task-independent metric for generative models in smart grid:** To our best knowledge, this is first-of-its-kind introduction of the Fréchet Power-Scenario Distance (FPD) in the smart grids context. FPD is specifically developed and trained to assess the performance of generative models in the power system domain. It can effectively handle multi-timescale data and provides a unified standard for a diverse range of power system tasks.

The rest of the paper is organized as follows: Section II details the design of the proposed evaluation metrics; Section A introduces model training detail; Section IV demonstrates

the effectiveness of FPD across various disturbances and its advantages over traditional metrics; and Section V concludes the paper.

II. DESIGN OF EVALUATION METRICS

A. Overview of the feature extraction model

We employ neural networks to extract high-level features capable of capturing complex spatial and temporal relations. Currently, a general feature extractor for this task does not exist in the power system domain. Implementing such a general model is challenging due to the diverse time resolutions and durations inherent in power system data. To address this challenge, we build a unified feature extraction framework that accommodates such diversity. As shown in Fig.1, our proposed framework is a multi-resolution multi-duration model, where a series of feature extractors, each trained for a specific time resolution, are interconnected hierarchically. This design allows multiple extractors to be combined for different data durations, with output features from each higher-resolution extractor feeding into the input of the subsequent lower-resolution extractor. This integration of high-resolution features into lower-resolution modules allows for effective utilization of detailed data in lower-resolution models without significantly increasing dimensional complexity.

B. Hierarchical feature extraction model

Considering the different timescales underlying the steady-state and transient-state data in power systems, we proposed two types of feature extraction models respectively. Due to the different sampling intervals, there are multiple resolutions and durations in steady-state data. Therefore, we adopt a multi-layer hierarchical architecture. For the transient-state situations, the sample intervals are much simpler, typically a selection of integer multiples of the rated frequency. Hence, we designed a single-layer model for the transient-state case.

The steady-state model can process time-series data with different resolutions $\{r_s\}$. The resolution progresses sequentially as follows:

$$r_s \in \{5\text{-min} \rightarrow \text{hourly} \rightarrow \text{daily} \rightarrow \text{monthly} \rightarrow \text{yearly}\}.$$

To accommodate steady-state data in different resolutions and durations, we employ a multi-layer structure. Each layer is designed to process data at a specific resolution r_s and transform it into a feature space aligned with the next higher resolution r_{s+1} . We denote the extractor handling data at resolution r_s as $\mathcal{M}_{r_s}(x_{r_s})$, where x_{r_s} represents data from the r_s resolution. Each encoding function \mathcal{M}_{r_s} takes an input x_{r_s} . The extractor then outputs a feature representation z_{r_s} for the next resolution r_{s+1} model processing.

We employ these extractors in different resolutions in a hierarchical structure, where each subsequent extractor builds upon the features aggregated from the stack of extractors in the prior level. A switch mechanism is introduced so that each extractor can adapt to the type of input it receives. Each extractor can select its input from either the features extracted at the prior resolution level, or the raw data at the current resolution level, as demonstrated in Fig.1. For instance, the

daily module (\mathcal{M}_{r_1}) can directly process 24 hourly data points if only hourly data is available, producing hourly features on a daily scale. Alternatively, if only 5-minute data is available, 24 hourly modules (\mathcal{M}_{r_0}) can be used to transform the 5-minute data for each hour (consisting of 12 data points per hour) into corresponding hourly features. Subsequently, the resulting 24 hourly features are concatenated and utilized as input to the daily module.

It is noteworthy that this structure has the capability to adapt multi-resolution, multi-duration data. The input data can be injected at any designated *entry* point in the model, depending on the data resolution r_s . The model will process the data through a series of lower-level extractors to higher-level extractors and finally generate the desired feature representation at the module corresponding to the target scale r_e .

During training and usage, the model processes the data in the form $\left(\frac{N}{L_{r_s}}, D_{r_s}, L_{r_s}\right)$ given the resolution of data r_s . Here, N denotes the total number of data points across all sequences. For example, consider 1,000 data samples, each representing daily-scale data recorded at 5-minute intervals. Since one day has 288 such intervals, the total number of data points is $1,000 \times 288 = 288,000$. L_{r_s} is the number of data points required at resolution r_s to form a single data point at the next higher resolution r_{s+1} ; for example, for 5-min resolution data, $L_{5\text{-min}} = 12$. Therefore, to process the entire batch of sequences, the dataset must be divided into segments of size $\frac{N}{L_{r_s}}$. Under this setup, $\frac{N}{L_{r_s}}$ modules \mathcal{M}_{r_s} will each handle a segment of length L_{r_s} , which aligns with the module design in our structure. Next, we define D_{r_s} as the augmented feature dimension associated with resolution r_s . This dimension includes features extracted from the preceding module, as well as a one-dimensional mean-value derived from the prior-level data. In contrast, the raw time-series data remain one-dimensional. In this case, the higher-level data is viewed as the mean-value of the lower-level data values, and the other lower-level extracted features can be simply zero-padded. This dimension, D_{r_s} , needs to be chosen properly so that feature space distribution is approximately Gaussian distributed because the subsequent Fréchet Distance calculation assumes that the features follow a Gaussian distribution.

Mathematically, to extract feature vectors for input data x_{r_s} at resolution r_s over a target duration r_e , we define the feature extraction process as a sequential operation within the hierarchical framework. The feature output at each resolution can be expressed as:

$$z_{r_s} = \mathcal{M}_{r_s}(\mathbf{I}_{r_s}), \quad (1)$$

where \mathbf{I}_{r_s} indicates the input at level r_s :

$$\mathbf{I}_{r_s} = \begin{cases} [z_{r_{s-1}}, \bar{x}_{r_{s-1}}], & \text{if } z_{r_{s-1}} \text{ is available} \\ [0, x_{r_s}], & \text{if } x_{r_s} \text{ is available} \end{cases}$$

In each resolution, we first determine input \mathbf{I}_{r_s} between the feature representation from the prior level and the data at the current level. Due to the dimensional inconsistency between $[z_{r_{s-1}}, \bar{x}_{r_{s-1}}]$, which has dimension D_{r_s} , and x_{r_s} , which has dimension 1, we need to pad x_{r_s} , if necessary, to match the dimension D_{r_s} . This operation ensures that all choices of \mathbf{I}_{r_s}

have the same dimension and can be adapted by the model. Also, considering the days in different months are inconsistent, for $r = 2$, we pad the length to 31 if needed. Then we reshape the \mathbf{I}_{r_s} to size $\left(\frac{N}{L_{r_s}}, D_{r_s}, L_{r_s}\right)$. This operation allows each module at a given resolution to process only a segment of the entire input sequence. Then, by stacking multiple such modules together, we ensure that the entire sequence in r_e scale is effectively processed. The reshaped feature vector z_{r_s} is passed as input to the extractor at the resolution r_{s+1} . We then update the resolution to $r_s = r_{s+1}$ and repeat this process sequentially until target resolution r_e is reached. Once r_e is achieved, we output the resulting feature vectors, which can be used to calculate the FPD score.

The parameters and modules corresponding to each resolution r are listed in Table I. The feature extraction algorithm is outlined in Algorithm 1.

TABLE I: Parameters and modules in steady-state model

i	r_i	D_{r_i}	L_{r_i}	\mathcal{M}_{r_i}
0	5-min	1	12	Hourly Module
1	Hourly	10	24	Daily Module
2	Daily	14	31	Monthly Module
3	Monthly	20	12	Yearly Module
4	Yearly	—	—	—

Algorithm 1 Feature Extraction Algorithm

- 1: **Input:** Duration r_e , Start resolution r_s , Batch size N , Input data x_{r_s} , Feature dimension D_{r_s} , Data Length L_{r_s} at resolution r_s
 - 2: **Output:** Final feature representation for data x_{r_s} in r_e scale
 - 3: **while** $r_s < r_e$ **do**
 - 4: **if** r_{s-1} is available **then**
 - 5: Set \mathbf{I}_{r_s} to $[z_{r_{s-1}}, \bar{x}_{r_{s-1}}]$
 - 6: **else if** r_s is available **then**
 - 7: Set \mathbf{I}_{r_s} to $[0, x_{r_s}]$
 - 8: **end if**
 - 9: Reshape \mathbf{I}_{r_s} to size $\left(\frac{N}{L_{r_s}}, D_{r_s}, L_{r_s}\right)$
 - 10: Calculate feature representation: $z_{r_s} = \mathcal{M}_{r_s}(\mathbf{I}_{r_s})$
 - 11: Advance resolution: $r_s = r_{s+1}$
 - 12: **end while**
 - 13: **Return** Output final feature vector z_{r_s}
-

The architecture designs are simpler in the transient-state cases. For this case, we use a single-time resolution with a 120Hz sampling frequency. Hence, we only apply a single feature extractor to the transient-state related task. A data sample is an 8-second length sequence with three channels of voltage magnitude, phase angle, and frequency, all represented in per-unit form. The input is first upsampled to 32 channels and finally downsampled by stride of 2 filters to a feature vector with 2048 dimensions. Then, we can calculate the FPD scores based on the extracted feature vectors.

For the architecture design of a single feature extractor in both models, we utilize residual blocks in the feature extractor

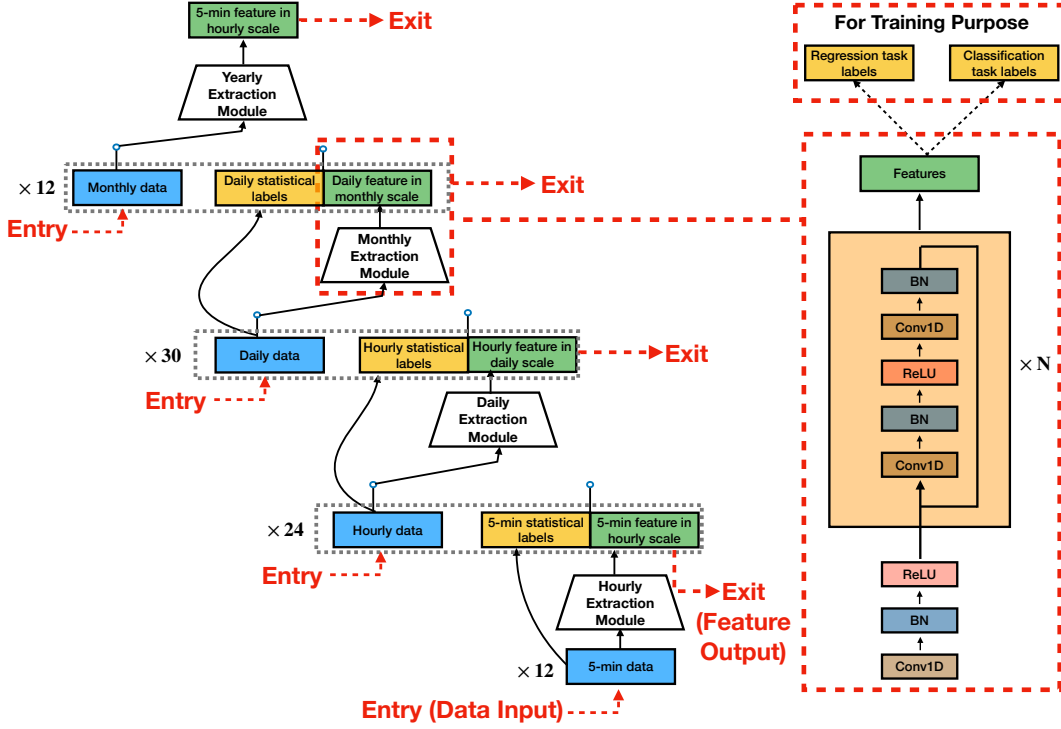


Fig. 1: Overview of the hierarchical multi-resolution feature extraction framework, integrating multiple time-scale feature extractors to enhance generative model evaluation in power systems.

as demonstrated in Fig.1. The residual connections have been widely studied and proved to increase neural network depth to enhance representation capabilities. We utilize the *conv-1d* and *batchnorm-1d* layers for accommodating the time-series inputs. This Resnet-like feature extractor is a base component for different scenarios and timescale tasks, followed by simple linear heads for different downstream training objectives.

C. Fréchet Power-Scenario Distance (FPD) calculation

Once robust representations are obtained from the feature extractor, we can then compare the distribution similarity between the two datasets in the feature space. Three distribution evaluation metrics have often been adopted [7]: (1) KL-divergence, (2) Kernel Distance (Maximum Mean Discrepancy - MMD), and (3) Fréchet Distance (Wasserstein-2 Distance).

The features can often be approximately viewed as having a Gaussian distribution. Denote the feature vectors extracted from two sets x_r^1 and x_r^2 at resolution r as z_r^1 and z_r^2 . The means of extracted features can then be expressed as:

$$\mathbf{m}_1 = \frac{1}{N} \sum_{i=1}^N z_{r,i}^1, \quad \mathbf{m}_2 = \frac{1}{N} \sum_{i=1}^N z_{r,i}^2 \quad (2)$$

The covariance matrices of the feature vectors extracted are:

$$\Sigma_1 = \frac{1}{N} \sum_{i=1}^N (z_{r,i}^1 - \mathbf{m}_1) (z_{r,i}^1 - \mathbf{m}_1)^T \quad (3)$$

$$\Sigma_2 = \frac{1}{N} \sum_{i=1}^N (z_{r,i}^2 - \mathbf{m}_2) (z_{r,i}^2 - \mathbf{m}_2)^T \quad (4)$$

Using the KL-divergence as the evaluating metric, the similarity between z_r^1 and z_r^2 can be assessed as [15]:

$$\text{KL}(z_r^1 || z_r^2) = \frac{1}{2} \left(\text{Tr}(\Sigma_2^{-1} \Sigma_1) + (\mathbf{m}_2 - \mathbf{m}_1)^T \Sigma_2^{-1} (\mathbf{m}_2 - \mathbf{m}_1) - d + \log \left(\frac{\det(\Sigma_2)}{\det(\Sigma_1)} \right) \right), \quad (5)$$

where d is the dimensionality of the feature space z_r^1 and z_r^2 . It is important to note that when applying the KL-divergence to compare the distance between two normal distributions, both z_r^1 and z_r^2 must have the same dimensionality. Because our goal is to design a metric that can compare datasets in different resolutions which have different feature dimensions, the KL-divergence is not suitable for our purpose. It is also well known that the KL divergence has the disadvantage of being asymmetric and unstable in some cases.

With the Kernel Distance as the evaluation metric, the distance between z_r^1 and z_r^2 is calculated as:

$$\begin{aligned} \text{MMD}(z_r^1, z_r^2) = & \|\mathbf{m}_1 - \mathbf{m}_2\|^2 + \frac{1}{N^2} \sum_{i=1}^N \sum_{j=1}^N \left(k(z_{r,i}^1, z_{r,j}^1) \right. \\ & \left. + k(z_{r,i}^2, z_{r,j}^2) - 2k(z_{r,i}^1, z_{r,j}^2) \right), \end{aligned} \quad (6)$$

where $k(x, y)$ is a kernel function (e.g., Gaussian kernel). Choosing a proper kernel is extremely important for the metric to be effective, as different kernel functions can lead to varying metric performance.

We propose to use the Fréchet Distance due to its stability and consistency as a metric based on our experiments. Since this metric is specifically tailored to evaluate power system scenarios, we name it Fréchet Power-Scenario Distance (FPD). The FPD(z_r^1, z_r^2) between the extracted features at resolution r is calculated as:

$$\text{FPD}(z_r^1, z_r^2) = \|\mathbf{m}_1 - \mathbf{m}_2\|^2 + \text{Tr}(\Sigma_1 + \Sigma_2 - 2(\Sigma_1 \Sigma_2)^{1/2}) \quad (7)$$

FPD is essentially a form of the Fréchet Distance, where we assume that the features of the two datasets follow Gaussian distributions. This metric quantifies the similarity between the two distributions: a smaller FPD value indicates a more significant similarity between the feature distributions, ultimately reflecting a higher similarity between the datasets.

III. MODEL TRAINING

The training data used in this study consists of multiple open-source datasets, each capturing different generative tasks. These datasets include various types of demand, EV charging profiles, and various types of electricity generation. Each dataset varies in terms of resolution and timescale, contributing to a comprehensive representation of the power system domain. The specific characteristics of each dataset are summarized in Table II.

For steady-state model, each module in the feature extraction model is trained individually and sequentially from the bottom level (5-min module) to the top level (yearly module). Once a certain level module has finished training, the parameters will be fixed, and we start to train the next level module. The training data for the module at each resolution is I_{r_s} . The training dataset is shown in Table II

Each module is trained based on the loss function:

$$L_{r_s} = \frac{1}{N} \sum_{i=1}^N \left[\sum_{k=1}^K (f_{\text{reg}}^k(I_{r_s}) - y_i^{\text{reg}})^2 - \sum_{i=1}^C y_i^{\text{clf}} \log(\text{softmax}(f_{\text{clf}}(I_{r_s}))) \right] \quad (8)$$

Both f_{reg} and f_{clf} are fully connected layers that take the feature output from the module and generate the corresponding predictions of tasks. Here, W denotes the layer weights, and b denotes the layer biases:

$$f_{\text{reg}}^k(I_{r_s}) = W_{\text{reg}}^k \mathcal{M}(I_{r_s}) + b_{\text{reg}}^k \quad (9)$$

$$f_{\text{clf}}(I_{r_s}) = W_{\text{clf}} \mathcal{M}(I_{r_s}) + b_{\text{clf}} \quad (10)$$

The first term in the (8), $\sum_{k=1}^K (f_{\text{reg}}^k(I_{r_s}) - y_i^{\text{reg}})^2$, corresponds to the Mean Squared Error (MSE) loss across a total of $K = 9$ regression tasks. Each regression task is designed for leading extractors to capture features that reflect a specific statistical characteristic of the data, represented by y_i^{reg} . The list of regression tasks is shown in Table V in Appendix. The second term, $-\sum_{i=1}^C y_i^{\text{clf}} \log(\text{softmax}(f_{\text{clf}}(I_{r_s})))$, represents the Cross-Entropy Loss for the classification task which categorize data based on classification labels y_i^{clf} . y_i^{clf} is determined by

the dataset index shown in Table II and C is the number of categories of dataset. The hyper-parameters for training are shown in Table VI in Appendix.

For transient-state model training, we employ the fault type, amplitude minimum, and maximum as supervised pretraining labels. We then exploit the pre-trained feature extractor to evaluate synthetic samples. The length of a data sequence is 960, and input data is encoded into a 2048-dimension representation. Moreover, the hyper-parameters for training are shown in Table VII in Appendix. Once training is complete, the tasks are irrelevant, and the obtained module $\mathcal{M}(I_{r_s})$ will be used for feature extraction.

All training and experiments were conducted on a 16 GB Apple M2 chip MacBook Pro. The model was trained using PyTorch 2.2, leveraging Apple's Metal Performance Shaders (MPS) backend for GPU acceleration.

IV. EFFECTIVENESS EVALUATION OF THE FPD

A. Effectiveness on different disturbances

In this section, we conduct several experiments to demonstrate the effectiveness of FPD. The experiments are designed based on the Wind Generation dataset 1 in Table II. We progressively increase the disturbance applied to the original dataset X in each experiment to provide a controllable and scalable measure of FPD performance.

- **Gaussian Noise:** In this case, Gaussian noise with a mean of 0 and a variance α is added to X . Where $\alpha \in [0, 0.16, 1.6, 4]$ represents the disturbance added. Larger α indicates more noise added.
- **Missing Data:** To simulate missing data points in X , we randomly replace some values with zeros for each sample in this case. The disturbance $\alpha \in [0, 0.1, 0.25, 0.5]$ indicates that $\alpha \times 100\%$ of the points in X are randomly set to zero.
- **Solar Data Contamination:** To show FPD can distinguish the data from another dataset, we contaminate the wind dataset X with data from the solar power dataset Y [17]. The disturbance $\alpha \in [0, 0.25, 0.5, 0.75]$ indicates that $\alpha \times 100\%$ of the samples in X are replaced by corresponding points from Y .
- **Gaussian Smooth:** To simulate scenarios where the generative model may fail to capture fine details of the original data, resulting in overly smooth outputs, we intentionally apply a Gaussian filter to blur these details. This operation allows us to test whether the FPD metric can detect such changes. The disturbance parameter $\alpha \in [0, 10, 20, 30]$ represents the standard deviation of the Gaussian filter applied to the original data, with higher values of α indicating more robust smoothing.
- **Error Accumulation:** Certain generative models, like Recurrent Neural Networks (RNNs), struggle with long sequences due to cumulative error over time. We introduce an accumulating error by applying Gaussian noise at each time step to simulate this effect. Specifically, for each time step t in sequence length T , we add a noise factor $\epsilon_t^{(\alpha)} \sim \mathcal{N}(1, \alpha)$ which is sampled from a Gaussian distribution centered at 1 with varying standard

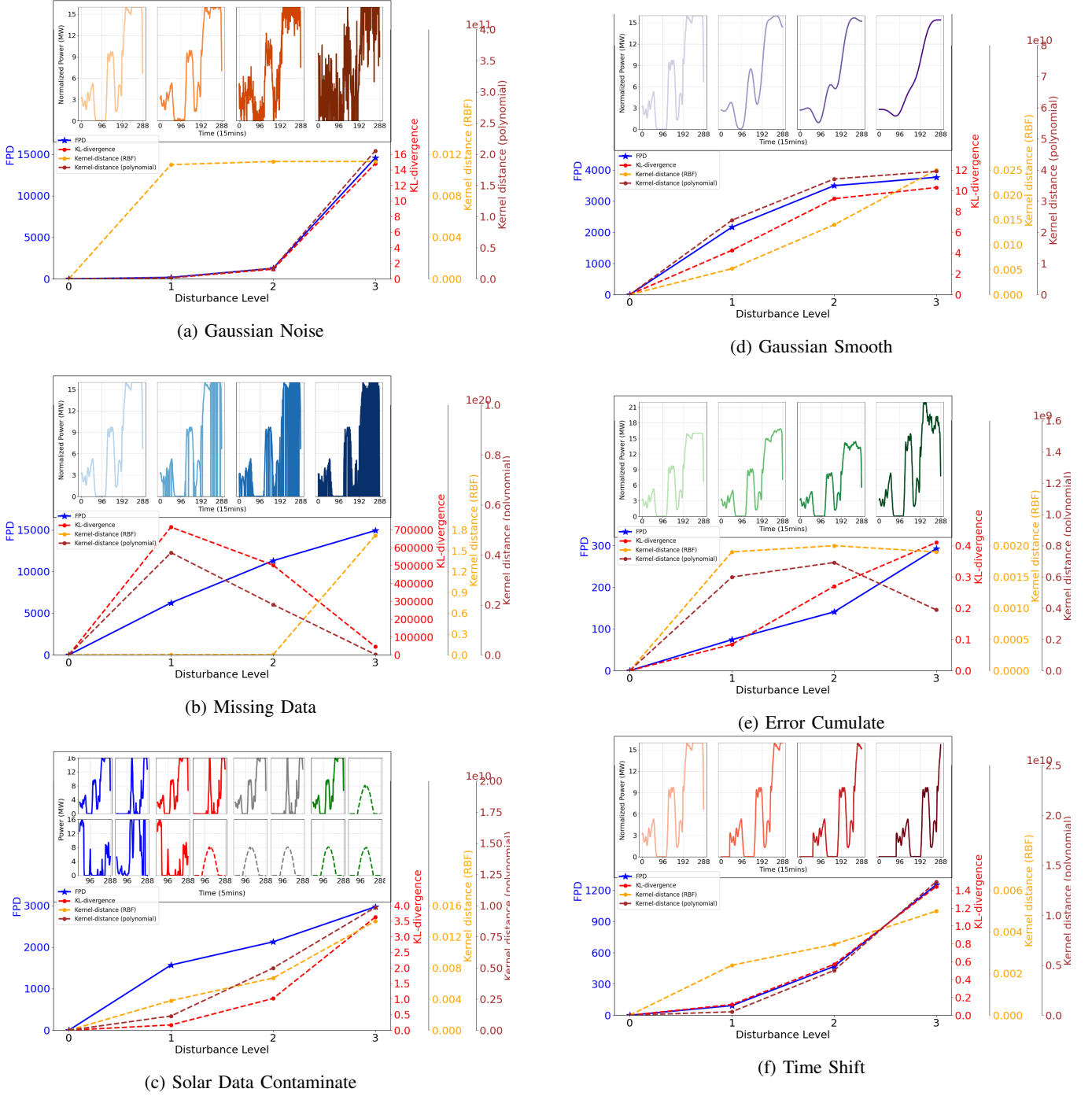


Fig. 2: Effect of six different types of disturbances on the dataset X : (2a) **Gaussian Noise** is added with mean 0 and varying variances $\alpha = [0, 0.16, 1.6, 4]$, where a larger α indicates more noise. (2b) **Missing Data** is simulated by randomly replacing $\alpha \times 100\%$ of the points in each sample of X with zeros, where $\alpha = [0, 0.1, 0.25, 0.5]$. (2c) **Solar Data Contaminate** replaces $\alpha \times 100\%$ of the points in X with corresponding points from a solar power dataset Y [17], where $\alpha = [0, 0.25, 0.5, 0.75]$. (2d) **Gaussian Smooth** applies Gaussian filter which has variance $\alpha = [0, 10, 20, 30]$ to the original dataset. Where a larger α indicates more significant smoothing. (2e) **Error Cumulate** is simulated by adding an error, which is times with a random Gaussian noise with a mean of 1 and varying variances $\alpha = [0, 0.005, 0.01, 0.03]$ at each time-step. (2f) **Time Shift** is a potential problem that exists in time-series generation. To simulate this effect, we shift the data forward by $\alpha = [0, 40, 60, 80]$ intervals.

TABLE II: Summary of Datasets Used for Training

Dataset	Description	Source	Resolution	Timescale
1	Wind Generation [16]	NREL	5-minute	1 year
2	Solar Generation [17]	NREL	5-minute	1 year
3	EV charging profiles [18]	Northwest Power and Conservation Council	Hourly	1 year
4	Commercial user load [19]	OpenEI.org	Hourly	1 years
5	Residential user load [19]	OpenEI.org	Hourly	1 years
6	Load Data in Texas [20]	ERCOT	Hourly	3 years
7	Demand by balancing authority [21]	EIA	daily	3 years
8	Generation by balancing authority [21]	EIA	daily	3 years
9	Utility Scale Electricity Net Generation [22]	EIA	monthly	14 years
10	Phasor Measurement Unit	PSSE simulations	0.016-second(60Hz)	50 hours

deviations, $\alpha = [0, 0.005, 0.01, 0.03]$. For each time step, we compute cumulative modification factors $E_t^{(\alpha)}$ recursively:

$$E_t^{(\alpha)} = E_{t-1}^{(\alpha)} \cdot \epsilon_t^{(\alpha)}, \quad E_0^{(\alpha)} = 1$$

The modified error cumulated data $\tilde{x}_t^{(\alpha)}$ is then given by:

$$\tilde{x}_t^{(\alpha)} = x_t \cdot E_t^{(\alpha)}$$

where x_t is the original data at time t . We demonstrate that the FPD metric effectively detects and highlights this error accumulation effect.

- **Time Shift:** Time shift in time-series data is a common issue in generative models, often leading to misalignment of temporal features between the original and generated data. This misalignment can be particularly problematic in power system data, where certain temporal features, such as peaks, carry critical information. To simulate this, we shift the data forward by intervals of $\alpha = [0, 40, 60, 80]$, creating misleading temporal dependencies. Our results demonstrate that FPD effectively detects and captures these temporal shifts.

As shown in Fig. 2, KL-divergence can be inconsistent due to its asymmetry feature, while Kernel Distance may fail to capture significant changes and is sensitive to kernel choice. Additionally, both methods also exhibit scale variability across disturbances. In contrast, Fréchet Distance consistently reflects disturbance levels and maintains stable scaling, making it a more reliable evaluation metric. For these reasons, we select Fréchet Distance as the evaluation metric and refer to our method as Fréchet Power-Scenario Distance (FPD).

B. Comparison of FPD with conventional evaluation metrics

1) *Sample-Wise Euclidean Distance (MAPE) vs. Distribution-Wise Distance (FPD):* Traditional Euclidean-based metrics such as Mean Absolute Percentage Error (MAPE) typically perform sample-wise comparisons, making the results highly dependent on the selection of sample pairs between the two datasets. This approach can lead to inconsistent and potentially invalid outcomes. To illustrate this, we revisit the Gaussian noise case presented in Fig. 2a. In this example, we make MAPE to match sample pairs randomly between the original and noise-perturbed datasets. As shown in Fig. 3, in some instances, higher noise levels result in lower MAPE values, which contradicts the ground truth. In contrast, the proposed FPD metric demonstrates expected behavior, providing a more effective measurement.

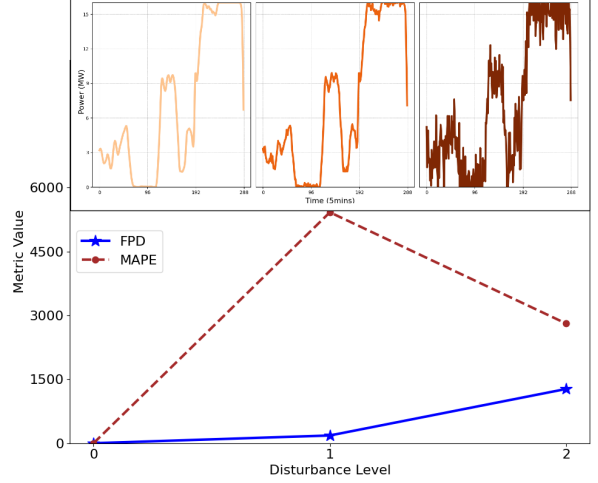


Fig. 3: Sample-wise distance MAPE VS. FPD

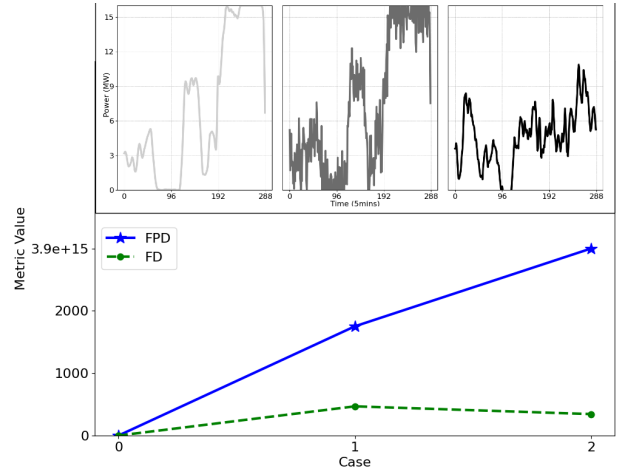


Fig. 4: Data-level Fréchet distance (FD) VS. FPD

2) *Data-Level Distribution Comparison (Fréchet Distance) vs. Feature-Level Distribution Comparison (FPD):* As previously noted, the data-level Fréchet Distance (FD) metric is often ineffective at capturing high-level complex patterns. FPD metric addresses this issue by incorporating feature extraction and measuring the similarity between distributions in the feature space. Feature extraction enables a better representation of higher-level patterns and structures within the data, allowing FPD to capture more relevant similarities for evaluating the

quality of generated data.

To demonstrate this advantage, we constructed a fabricated dataset by randomly sampling from a distribution with a similar mean and covariance to the original data. Despite these similarities, the fabricated dataset lacks the temporal patterns present in the original dataset, resulting in a sparse relation. As shown in Fig. 4, while FD fails to identify this disparity, FPD accurately reflects the weaker relationship between the fabricated and original datasets.

C. Coherence between FPD and the downstream tasks

To assess whether FPD's indication of high-quality data can be used to determine the practical usefulness for downstream tasks, we further evaluate its efficacy for transient-state case using PMU data containing three types of faults. We employ the Brownian noises to mimic the accumulating temporary errors in the PMU data prediction as depicted in Fig. 5. As shown in Table III, we cross-evaluate different fault scenarios. Hence, we can observe non-zero diagonal elements in the FPD score matrix, along with the diagonal values being significantly lower than the non-diagonal elements, showing the capability of identifying different scenarios other than evaluating generation quality. To further prove the capability of FPD can handle the downstream task in steady-state case, we reuse the wind dataset [16] and define the sub-task as data classification based on the average power across the day as used in Chen's work [23]. The three cases differ based on average power levels, as shown in Fig. 6. Moreover, the cross-evaluation of different mean value scenarios is shown in the Table.IV again highlights the alignment between the FPD evaluation and the specific sub-task.

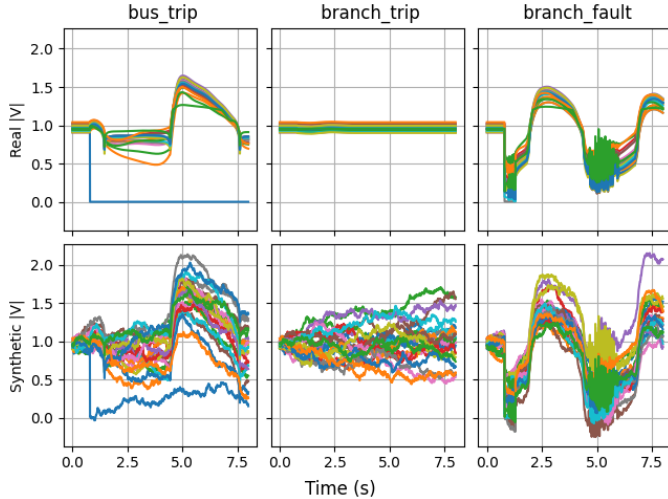


Fig. 5: Ground-truth and synthetic PMU voltage magnitude curves under different fault scenarios. Synthetic data is modulated using Brownian noises.

D. Cross-model comparison with FPD

In the previous sections, all evaluations were conducted directly on the artificially generated datasets. This approach enables precise control over generation quality and model

TABLE III: Cross-evaluation on FPD performance for PMU data.

Ground-truth $ V $ \ Synthetic $ V $	bus_trip	branch_trip	branch_fault
bus_trip	744.26	1086.07	2586.15
branch_trip	1462.24	846.03	2720.04
branch_fault	2516.35	2401.13	687.99

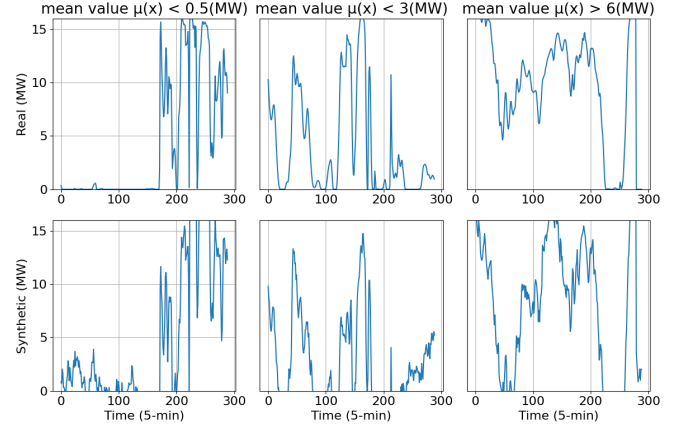


Fig. 6: Ground-truth and synthetic wind power under different mean scenarios. Synthetic data is modulated using Brownian noises.

performance assessment. However, FPD can also be used to evaluate model generated performing the same task, as demonstrated in the following two scenarios.

1) Scenario 1: EV Charging Profile Data Generation

Accurately evaluating the quality of synthetic data in real-world settings presents a significant challenge, as highlighted by [24], for which FPD provides a solution. [24] proposed a novel generative model, DiffCharge, based on a diffusion model designed to conditionally generate electric vehicle (EV) charging power profiles. Probability density function (PDF) comparisons and discriminative scores derived from a trained classifier were used to evaluate battery-level data generation performance between DiffCharge and baseline models such as Time-GAN. However, evaluations for station-level data generation were not given. We conduct experiments to compare DiffCharge's performance with a W-GAN model on the station level; see Fig. 7. We find that DiffCharge achieves a lower FPD score. Visually, we also observe that DiffCharge can capture the general trend better, while W-GAN generates less realistic peaky signals. Therefore, our results indeed support the conclusion that the DiffCharge model can more accurately approximate the distribution of EV charging profiles at both the station-level and battery-level.

2) Scenario 2: Wind Power Data Generation

To further demonstrate FPD's cross-model comparison ability, we replicate the study from [1], where the authors introduced a model called StyleGAN, which integrates forecast and climate data to enhance the generation of

TABLE IV: Cross-evaluation on FPD performance for wind power data.

Ground-truth MW \ Synthetic MW	$\bar{x} < 0.5$	$\bar{x} < 3$	$\bar{x} > 6$
$\bar{x} < 0.5$	736.97	1300.42	901.36
$\bar{x} < 3$	1300.42	565.35	2720.04
$\bar{x} > 6$	901.36	989.83	686.51

renewable energy data. They showed that StyleGAN is superior to WGAN proposed in [23] based on multiple uncertainty quantification and statistical metrics, such as RMSE. In our experiment, the differences between generations from StyleGAN and WGAN were challenging to distinguish through visual inspection. StyleGAN's results seemed to capture the overall trend more accurately. As shown in Fig. 8, FPD confirms StyleGAN aligns better with real data, supporting the findings in [1].

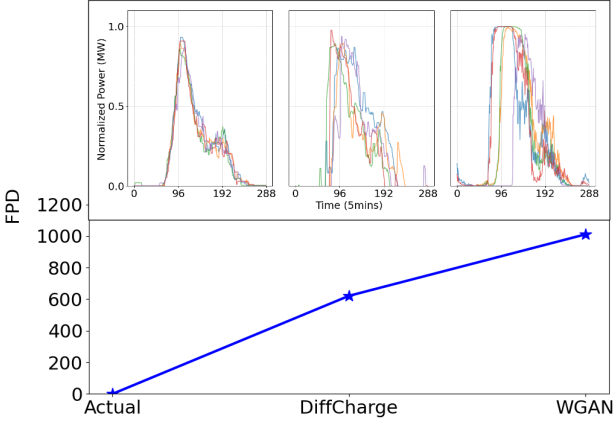


Fig. 7: **Scenario 1** – Comparison of DiffCharge and W-GAN in generating EV charging profiles at the station level.

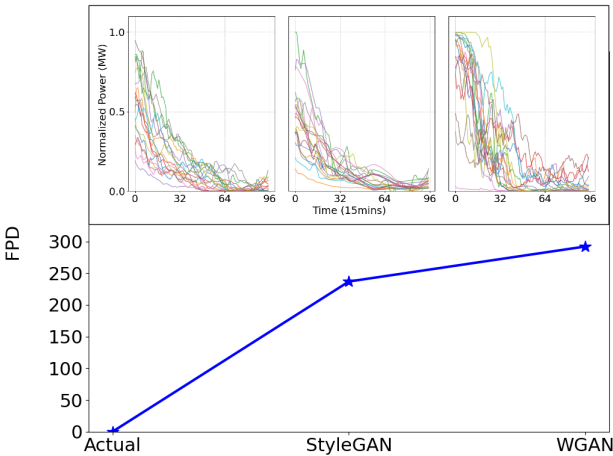


Fig. 8: **Scenario 2** – Comparison of W-GAN and StyleGAN in generating wind power data.

E. Comparability across varying time resolutions

A key feature of FPD is its ability to adapt to varying time resolutions within a single metric. This flexibility enables effective comparisons across datasets with different time resolutions. To demonstrate this capability, we collected hourly resolution data for solar and wind power and evaluated their similarity with the 5-minute resolution solar and wind power datasets used in Section IV-A. The results, shown in Fig. 9, indicate that FPD successfully identifies that the solar power datasets are more similar to each other than they are to the wind power data despite their differing time resolutions. This result demonstrates the metric's effectiveness in facilitating comparability across datasets with different temporal resolutions.

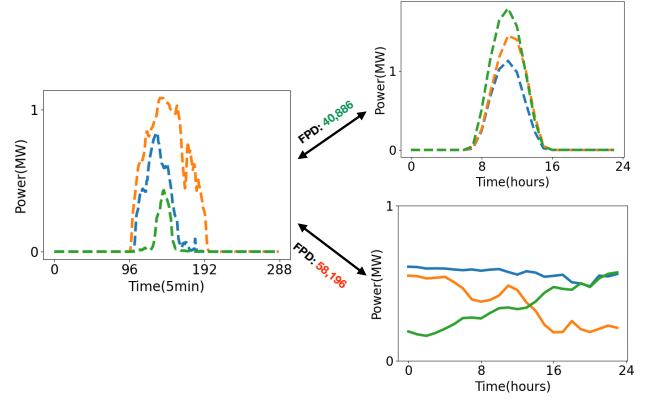


Fig. 9: The FPD metric is evaluated between the **left**: 5-min resolution solar power dataset [17], **right top**: hourly resolution solar power dataset [25] and **right bottom**: hourly resolution wind power dataset [25]. The results demonstrate that FPD effectively generalizes across different time resolutions.

V. CONCLUSION AND FUTURE WORK

This paper introduces the Fréchet Power-Scenario Distance (FPD) as a novel, task-agnostic metric for evaluating generative model outputs in the power systems sector. FPD addresses the limitations of traditional metrics by employing a hierarchical feature extraction framework that captures multi-resolution temporal information. Then, the Fréchet Distance is applied to assess the quality of generated data in the feature space. This method enables FPD to provide an accurate, robust, and consistent evaluation across diverse power system applications.

Comprehensive case studies demonstrate FPD's effectiveness in distinguishing data quality across various disturbances, time resolutions, and sub-task scenarios. These results underscore FPD's potential as a standardized cross-model approach for validating generative models, offering support for both enhancing model quality and promoting wider adoption within the power systems domain.

There are some potential studies for future work. 1) Currently, the dataset we are using is still limited due to accessibility constraints. Thus, building a more comprehensive dataset tailored to a wider range of tasks within the power system domain is possible to improve the performance of

FPD; 2) While the current model structure can handle multi-resolution and multi-duration data, it is not yet sufficiently generalized to accommodate data of any resolution or duration. Therefore, there is potential for developing a more generalized structure that can address this challenge and further enhance the versatility of the metric.

REFERENCES

- [1] Ran Yuan, Bo Wang, Yeqi Sun, Xuanning Song, and Junzo Watada. Conditional style-based generative adversarial networks for renewable scenario generation. *IEEE Transactions on Power Systems*, 38(2):1281–1296, 2022.
- [2] Adam B. Birchfield, Ti Xu, Kathleen M. Gegner, Komal S. Shetye, and Thomas J. Overbye. Grid structural characteristics as validation criteria for synthetic networks. *IEEE Transactions on Power Systems*, 32(4):3258–3265, 2017.
- [3] Nadjib Mohamed Mehdi Bendaoud, Nadir Farah, and Samir Ben Ahmed. Comparing generative adversarial networks architectures for electricity demand forecasting. *Energy and Buildings*, 247:111152, 2021.
- [4] Robbert Claeys, Rémy Cleenwerck, Jos Knockaert, and Jan Desmet. Capturing multiscale temporal dynamics in synthetic residential load profiles through generative adversarial networks (gans). *Applied Energy*, 360:122831, 2024.
- [5] Junkai Liang and Wenyuan Tang. Sequence generative adversarial networks for wind power scenario generation. *IEEE Journal on Selected Areas in Communications*, 38(1):110–118, 2019.
- [6] Yushan Liu, Zhouchi Liang, Xiao Li, and Abualkasim Bakeer. Generative adversarial network and cnn-lstm based short-term power load forecasting. In *2023 IEEE 17th International Conference on Compatibility, Power Electronics and Power Engineering (CPE-POWERENG)*, pages 1–6. IEEE, 2023.
- [7] Mina Razghandi, Hao Zhou, Melike Erol-Kantarci, and Damla Turgut. Variational autoencoder generative adversarial network for synthetic data generation in smart home. In *ICC 2022-IEEE International Conference on Communications*, pages 4781–4786. IEEE, 2022.
- [8] Han Liu, Xinyu Cao, Caitang Sun, and Gang Li. Methodologies of feature extraction for voltage sags in power system. In *2021 IEEE 2nd China International Youth Conference on Electrical Engineering (CIYCEE)*, pages 1–5. IEEE, 2021.
- [9] Simona-Vasilica Oprea, Adela Bâra, Florina Camelia Puican, and Ioan Cosmin Radu. Anomaly detection with machine learning algorithms and big data in electricity consumption. *Sustainability*, 13(19):10963, 2021.
- [10] Tim Salimans, Ian Goodfellow, Wojciech Zaremba, Vicki Cheung, Alec Radford, and Xi Chen. Improved techniques for training gans. *Advances in neural information processing systems*, 29, 2016.
- [11] Bhagyashree, Vandana Kushwaha, and G. C. Nandi. Study of prevention of mode collapse in generative adversarial network (gan). In *2020 IEEE 4th Conference on Information & Communication Technology (CICT)*, pages 1–6, 2020.
- [12] Martin Heusel, Hubert Ramsauer, Thomas Unterthiner, Bernhard Nessler, and Sepp Hochreiter. Gans trained by a two time-scale update rule converge to a local nash equilibrium. *Advances in neural information processing systems*, 30, 2017.
- [13] Mikołaj Bińkowski, Danica J Sutherland, Michael Arbel, and Arthur Gretton. Demystifying mmd gans. *arXiv preprint arXiv:1801.01401*, 2018.
- [14] Shane Barratt and Rishi Sharma. A note on the inception score. *arXiv preprint arXiv:1801.01973*, 2018.
- [15] John Duchi. Introduction to statistics: Gaussian distributions. https://stanford.edu/~jduchi/projects/general_notes.pdf. Accessed: 2024-10-21.
- [16] Caroline Draxl, Andrew Clifton, Bri-Mathias Hodge, and Jim McCaa. The wind integration national dataset (wind) toolkit. *Applied Energy*, 151:355–366, 2015.
- [17] National Renewable Energy Laboratory (NREL). Solar power data for integration studies (sind) toolkit, 2024. Accessed: 2024-10-04.
- [18] Northwest Power and Conservation Council. Plug-in electric vehicle load profiles. https://www.nwcouncil.org/2021powerplan_plug-electric-load-profiles/, 2021. Accessed: 2024-10-04.
- [19] GWU Big Data & Analytics Lab. Commercial and residential hourly load data set. <https://bigdata.seas.gwu.edu/data-set-11-commercial-and-residential-hourly-load-data-set/>, 2024. Accessed: 2024-10-04.
- [20] Electric Reliability Council of Texas (ERCOT). ERCOT Historical Load Data. https://www.ercot.com/gridinfo/load/load_hist/index.html. Accessed: 2024-10-04.
- [21] U.S. Energy Information Administration (EIA). Eia open data: Daily regional data for electricity. <https://www.eia.gov/pendata/browser/electricity/rto/daily-region-data>, 2024. Accessed: 2024-10-04.
- [22] U.S. Energy Information Administration (EIA). Electric power operational data. <https://www.eia.gov/pendata/browser/electricity/electric-power-operational-data>, 2024. Accessed: 2024-10-04.
- [23] Yize Chen, Yishen Wang, Daniel Kirschen, and Baosen Zhang. Model-free renewable scenario generation using generative adversarial networks. *IEEE Transactions on Power Systems*, 33(3):3265–3275, 2018.
- [24] Siyang Li, Hui Xiong, and Yize Chen. Diffcharge: Generating ev charging scenarios via a denoising diffusion model. *IEEE Transactions on Smart Grid*, 2024.
- [25] Open Power System Data. Time series, 2020. Version 2020-10-06.

APPENDIX

TABLE V: Regression labels for steady-state training

Regression Tasks
Minimum
Maximum
Range
Variance
Number of data points above average
Number of data points below average
Skewness
Kurtosis
Coefficient of variation

TABLE VI: Hyper-parameters for steady-state model training

Parameter	Setting
Minibatch size	1024
Optimizer	Adam
Optimizer: learning rate	1e-3

TABLE VII: Hyper-parameters for transient-state model training

Parameter	Setting
Minibatch size	128
Optimizer	Adam
Optimizer: learning rate	1e-4
Optimizer: weight decay	2e-5
Classification loss coefficient	1.0
Regression loss coefficient	1.0